Article

Journal of Intelligent Material Systems and Structures

Journal of Intelligent Material Systems and Structures
23(18) 2077–2093

DOI: 10.1177/1045389X12443015
jim.sagepub.com
SAGE

Multi-objective optimal control of vibratory energy harvesting systems

Jeff T Scruggs[1], Ian L Cassidy[2] and Sam Behrens[3]

Abstract

This article examines the use of actively controlled electronics to maximize the energy harvested from a stationary stochastic disturbance. In prior work by the authors, it has been shown that when the harvester dynamics are linear and the transmission losses in the electronics are resistive, the optimal feedback controller is the solution to a nonstandard linear-quadratic-Gaussian optimal control problem. This article augments the theory in the following three distinct ways: (a) It illustrates how to use linear matrix inequalities to balance the objective of energy harvesting against other response control objectives (such as minimum requirements on closed-loop damping and maximum levels of voltage response), in the synthesis of the optimal feedback law; (b) it establishes a more realistic characterization of the transmission losses in the actively controlled power electronics used to regulate the extraction of power; and (c) it illustrates how the optimal control theory for resistive loss models can be extended to accommodate the more realistic loss models. The theory is illustrated in the context of a piezoelectric energy harvesting model, and an example is used to illustrate that the theory can be used to simultaneously optimize the feedback law, together with the switching frequency and storage bus voltage of the power electronics.

Keywords

control, energy harvesting, optimization

Introduction

Vibratory energy harvesting has been the subject of considerable engineering research, with applications over a wide range of scales and in many technological domains. The particular technologies employed for transduction, power processing and control, and energy storage vary for different power and time scales. Much of the more recent research has focused on harvesting milliwatt-scale power from ambient structural vibrations (Beeby et al., 2006; Priya and Inman, 2009). For excitation frequencies above about 10 Hz, piezoelectric transducers have been the predominant transduction technology, although electromagnetic and electrostatic transduction technologies have also been demonstrated to be effective and promising (Anton and Sodano, 2007). For larger structural vibration applications, at the 1–100 W scale and at frequencies of 1 Hz and below, a number of researchers have investigated the use of permanent-magnet machines as generators, both in back-driven rotary (Cassidy et al., 2011; Nagode et al., 2010) and linear direct (Zuo et al., 2010) realizations. Finally, at power scales on the order of 100 kW and beyond, and at frequencies in the range of 0.075–0.2 Hz, ocean wave energy converters have been investigated for decades, using transduction technologies including (but not limited to) direct-drive permanent-magnet machines as well as hydraulic pumps (Cruz, 2008).

Figure 1 illustrates a conceptual diagram of a multi-port energy harvester. We consider an electromechanical system in which n_p transducer ports are embedded, with transducer k associated with a voltage v_k and current i_k. (When a harvester has more than one transducer port, we refer to the vectors of these quantities as v and i.) The system is excited by one or more external disturbances, which we denote by a. (In the case where more than one disturbance exists, a is also a vector.) The electromechanical system, which we call the "harvester," is the conduit that transfers vibratory energy

[1]Department of Civil and Environmental Engineering, University of Michigan, Ann Arbor, MI, USA
[2]Department of Civil and Environmental Engineering, Duke University, Durham, NC, USA
[3]Commonwealth Scientific and Industrial Research Organization (CSIRO) Energy Centre, Newcastle, NSW, Australia

Corresponding author:
Jeff T Scruggs, Department of Civil and Environmental Engineering, University of Michigan, 2340 GG Brown Laboratory, 2350 Hayward Street, Ann Arbor, MI 48109, USA.
Email: jscruggs@umich.edu

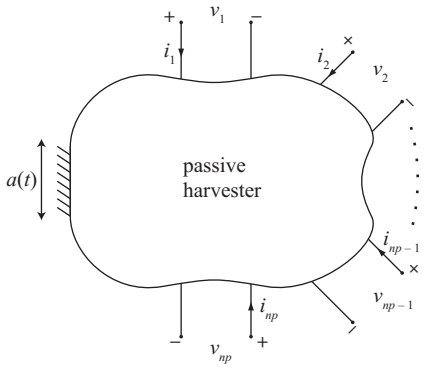

Figure 1. Generic multiport harvester.

from the excitation to the transducer terminals, where its extraction and transmission are regulated via the use of electronics. In many smaller scale energy harvesting applications, it is comprised of a resonant piezoelectric system (such as a unimorph or bimorph beam), with each voltage corresponding to a different piezoelectric patch. However, the model may also apply to electromagnetic harvesters, which are often comprised of simple single-degree-of-freedom inertial resonators, in which case a voltage v_k would correspond to the open-circuit back-electromagnetic force (EMF) of an electromagnetic transducer.

The problem of optimizing generation of energy from piezoelectric harvesters, under various assumptions for the nature of excitation a, has been examined by many researchers. In this introduction, we review some of the contributions to this area. This is not intended to be an exhaustive survey but rather an overview of some of the highlights of recent work. The focus is on small-scale applications.

The case in which a is sinusoidal with known frequency has received by far the most attention. Typically, the harvester's natural frequency is tuned to coincide with the disturbance frequency. This creates sizable open-circuit voltages v, which in many studies are interfaced with a storage device (such as a rechargeable battery of supercapacitor) via a passive diode bridge rectifier (Amirtharajah and Chandrakasan, 1998; Roundy et al., 2002), as illustrated in Figure 2(a) for a single transducer. This approach is advantageous because it is an entirely passive system, but has two limitations. First, the voltage v will only connect to the supply voltage bus V_S when the diode bridge is forward biased, which means that power can only be generated when $|v|>V_S$. Second, when power does flow from transducer to storage, there is no direct way to control of this power flow. In the absence of such control, the circuit may in some circumstances impose excessive damping on the harvester, which in turn suppresses the transducer voltage, and results in a very low power.

Motivated by such observations, a number of researchers have proposed the use of high-frequency

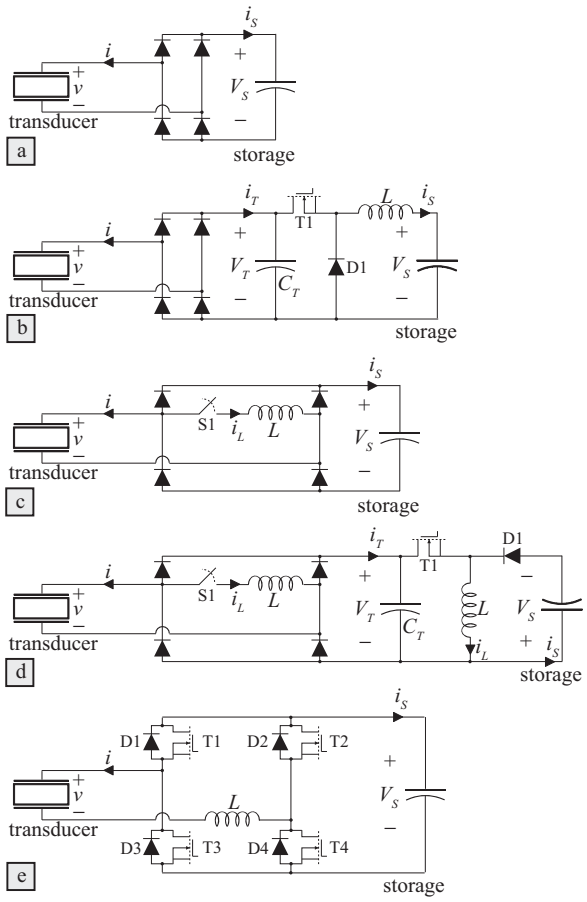

Figure 2. Power conditioning circuits: (a) passive diode bridge rectifier, (b) PWM-switched controllable DC/DC (buck) converter, (c) SSHI circuit with passive rectifier, (d) SSHI circuit with controllable DC/DC (buck–boost) converter, and (e) PWM-switched controllable bidirectional H-bridge.
PWM: pulse-width modulation; SSHI: synchronized-switched harvesting on inductor.

PWM-switched DC/DC converters to control power extraction from harvesters (Kasyap et al., 2002; Taylor et al., 2001). Figure 2(b) illustrates the converter proposed by Ottman et al. (2003), which is a buck converter. By operating the converter in discontinuous conduction with a constant duty cycle D, they observed that the low-frequency impedance of the electronics, as seen from the terminals of the transducer-side capacitor C_T, is insensitive to the voltage magnitude V_T, assuming $V_T \gg V_S$, and is approximately resistive under these circumstances. This gave rise to the observation that a single duty cycle D (thus yielding a constant input resistance) is near-optimal for any level of excitation for which $|v| \gg V_S$ is satisfied most of the time. When thus operated, the circuit is analogous to the passive rectifier in Figure 2(a), but with the difference that V_S is now V_T. Crucially, V_T is the voltage across a capacitance in parallel with the input resistance of the converter, and therefore will rise and fall with the average levels of $|v|$, resulting in response behavior that is near-

homogeneous across a range of excitation levels. Moreover, the rate of power extraction can be readily controlled by adjusting the duty cycle D to vary the effective resistance.

Since that study, a number of subsequent researchers have investigated the use of other PWM converter topologies to regulate power extraction. Lefeuvre et al. (2007) point out that the discontinuously conducting buck–boost converter is the topology that results in an input resistance, which is (theoretically) completely invariant as the magnitude of v varies, irrespective of the value of V_S. Further studies by Kong et al. (2010) have expanded on this observation. Through these studies, it has become clear that by controlling these converters at constant duty cycle, with an appropriately small transducer-side capacitance C_T, one can create an energy storage recharge circuit that extracts power as if it were a linear resistor.

This is important, because as has been observed by many researchers (Scruggs, 2010; Shu and Lien, 2006; Stephen, 2006), the theoretically optimal power extraction from a monochromatically excited linear energy harvester is attained by connecting the harvester to a recharge circuit that has a linear input impedance (assuming the transmission losses in the circuit can be neglected). Specifically, this optimal impedance is matched to the complex conjugate (for the multitransducer case, complex conjugate transpose) of the harvester's driving point impedance as measured from the transducer terminals. As such, for single-transducer applications, the optimal harvesting circuit is comprised of a linear resistor together with (in series or parallel) a reactive component. Depending on the transducer technology and the frequency of excitation, this reactive component will either be an inductor or a capacitor. As such, impedance matching theory leads us to the conclusion that if one ignores practical considerations (such as parasitic losses in the electronics, sizes of various electrical components, and parametric uncertainty), there is a clear "optimal" energy harvesting circuit for single-transducer linear harvesters subjected to monochromatic excitation—it is always a discontinuously conducting buck–boost converter driven at constant duty cycle, in combination with a passive linear reactance.

Piezoelectric transducers responding at resonance exhibit a sizable internal capacitive reactance, resulting in a very low power factor (i.e. cosine of the phase angle between the velocity-proportional internal current source for the transducer's Norton equivalent circuit, and its open-circuit voltage). The reactive component of the matched impedance thus turns out to be an inductance, the value of which can be hundreds of Henries; orders of magnitude too large to be implemented on a small-scale application. Efforts to implement power factor correction in piezoelectric applications, while requiring smaller inductors, have given rise to the various nonlinear synchronized-switched harvesting on inductor (SSHI) circuits. Figure 2(c) illustrates the "parallel SSHI" circuit, examined in Badel et al. (2005), Guyomar et al. (2005), and Lefeuvre et al. (2005), and in many subsequent studies (see Wickenheiser and Garcia (2010) and Lien et al. (2010) for recent reviews of the rapidly evolving literature on SSHI circuits.) The circuit operates by closing the parallel switch every time a peak in transducer displacement is detected. Each time the switch closes, this causes the L–C circuit formed by the switched inductor and the piezocapacitance to quickly oscillate through one half-cycle. (Typically, L is chosen to be small enough that the period of this half-cycle is considerably shorter than the excitation period.) At the end of the half-cycle, the inductor demagnetizes, and this triggers the switch to open again, and remain so until it is again triggered by a subsequent displacement peak. The effect of the switching operations is therefore to force a near-instantaneous reversal of the magnitude of voltage v, thus causing v to exhibit zero crossings at approximately the same times as the transducer velocity. As such, the fundamental harmonic of power generation (i.e. at the excitation frequency) exhibits an effective power factor close to unity. However, unlike the linear impedance-matched circuit, the inductance necessary to implement SSHI circuits is only limited by practical considerations, such as ratings on peak current and dissipation.

SSHI circuits have been investigated for interface with both diode bridge rectifiers as in Figure 2(c) (Liang and Liao, 2011) and to interface with the effective input resistance of a buck–boost DC/DC converter, as illustrated in Figure 2(d) (Kong et al., 2010). The effective resistance (and therefore the duty cycle) of the converter in Figure 2(d) should be chosen in a similar manner as it would in a linear impedance-matched circuit. Almost all SSHI techniques have presumed harmonic excitation.

Liu et al. (2009) point out that SSHI circuits have a disadvantage, in that during the time when the inductor is switched on, i_L is uncontrollable, and the only way to adjust the design to bound its peak value is to increase L. However, increasing L also slows the voltage reversal time. Large values of i_L lead to higher root mean square (RMS) losses for the circuit, and thus, there is an advantage to a circuit that can more carefully regulate current during the voltage reversal, while still yielding fast reversal times. Toward this end, Liu et al. advocate the use of a fully active PWM-controlled H-bridge circuit, as illustrated in Figure 2(e), which allows for full control of the current i. The circuit is bidirectional, meaning that power may be made to flow both ways through the converter (i.e. from v to V_S as well as the other way). During times when an actual SSHI switch would be open, the diode bridge in the H-bridge circuit is forward biased (i.e. $|v|>V_S$) and power flows

to storage. During the brief periods when the SSHI switch would be closed, the H-bridge is controlled to draw a large constant current from the transducer, causing the voltage of the piezoelectric to reverse its sign with approximately linear rate of change. During the first half of the reversal action, the H-bridge extracts charge from the piezocapacitance, resulting in power flow from v to V_S. During the second half, the H-bridge pumps energy back into the piezocapacitance, resulting in power flow from V_S back to v, until $|v|$ has increased to V_S again. At this time, the diode bridge in the H-bridge becomes forward biased, and the effective SSHI switch becomes open again. As such, the advantage of implementing "artificial" SSHI with an H-bridge is that the maximum current during the switching operations can be regulated, and also that the voltage reversal times can be minimized subject to this maximum current restriction.

As with the single-directional DC/DC converters in Figure 2(b) and (d), current control in an H-bridge is accomplished via high-frequency PWM switching. By appropriate switching of its four metal–oxide–semiconductor field-effect transistors (MOSFETs), the H-bridge can be controlled to raise or lower the current i arbitrarily to track a desired value, and because L is typically designed to be small, current tracking can be effected at high bandwidth. As such, H-bridges require an electronic controller and require that the four distinct MOSFETs be gated at high frequency. Consequently, the suitability of the circuit depends on the power scale of the application, and how this compares with technological details relating to parasitic losses associated with electronic control.

Considerable research has extended many of the ideas discussed earlier to the case in which the frequency of excitation changes slowly and in a manner which is uncertain. Recently, Cammarano et al. (2010) illustrated that the synthetic harvesting impedance for the electronics can be adapted to these changes, as the excitation shifts away from resonance of a harvester, in order to maintain theoretical impedance matching conditions. The practicalities of adapting the reactive component of a impedance-matched circuit would likely require active control with a bidirectional electronic converter, such as the H-bridge discussed earlier, although SSHI circuits with appropriate phase-shifting can also be used for this purpose (Luo and Hofmann, 2011). It should also be noted that considerable research has focused on the use of nonlinearity and also the use of multiple transducers to create energy harvesting systems for narrowband disturbances, which are robust to large uncertainties in the disturbance frequency (see Tang et al. (2010) for a recent synopsis of the many efforts in this area).

In many applications, the disturbance a cannot be presumed to be narrowband and is much more appropriately modeled as a stochastic process, possibly with a low quality factor. For such cases, determination of the optimal energy harvesting circuit is more challenging because the system must harvest energy from a continuous band of frequencies *simultaneously*. It should be noted that this problem is fundamentally different from the aforementioned problem in which the disturbance is assumed to be monochromatic but with uncertain frequency. Indeed, it may be the case that a system optimized for one of the two problems performs poorly when applied to the other. Halvorsen (2009) investigated the broadband energy harvesting problem, in which he modeled a as white noise and investigated R–L–C networks to extract power from electromagnetic and piezoelectric transducers. This research was followed up by Adhikari et al. (2009), who performed a similar analysis and examined related optimization of these networks. Daqaq (2011) examined the influence of nonlinearity on stochastic energy harvesting, pointing out the interesting fact that for white-noise-excited single degree-of-freedom systems with nonlinear stiffness (and minimal transducer reactance), the optimal harvesting circuit still has a linear input resistance. However, this is not true for the case of colored noise excitation.

Simultaneously with the above-mentioned research, Scruggs (2009) showed that for white-noise-excited harvesters, the optimal causally attainable power generation (i.e. the power generation achievable without knowing the disturbance ahead of time) is achievable only with active control, that is, with a bidirectional active drive circuit such as H-bridge. Furthermore, the determination of the optimal power extraction can be framed as a feedback optimization problem, with the optimal feedback being determined via the solution to an associated linear-quadratic-Gaussian (LQG) control problem. In Scruggs (2010), this analysis is extended to the case of colored disturbance noise of arbitrary quality factor. These studies illustrate that when the drive electronics are efficient enough, the frequency content of the optimized power flow is such that in frequency bands near resonance, average power flows from transducer to storage, but in other frequency bands, average power flows the other way. This implies that the optimal harvesting circuit cannot be made equivalent to any passive network, as is done for harmonic energy harvesting via impedance matching theory. These studies also showed that in a stochastic context, the causal limit on the average harvested power is due to limitations on energy conversion efficiency as well as information-related limitations arising from an inability to accurately ascertain the internal state of the harvester.

The present article further explores the connections between optimal feedback control theory and energy harvesting. The analysis is conducted in a stochastic context and assumes an active power-electronic drive as in Figure 2(e). We presume the active drive is operated in discontinuous conduction, the operation and modeling of which are discussed at length in "Nonquadratic

loss model of an H-bridge." At present, it suffices to say that what this accomplishes is the ability of the harvesting circuit to track a desired current with high bandwidth, based on feedback of the transducer voltage v. Specifically, the contributions of the article are as follows:

1. We develop a detailed model for the losses in the electronics, including gating, transition, diode, and resistive loss types, and show how these losses affect the determination of the optimal feedback law. We also show how the choice of storage bus voltage (V_S) and PWM switching frequency affect the optimal controller and the optimized power.
2. We show how the objective of energy harvesting can be balanced against other competing objectives that are necessary for the drive to operate properly. Specifically, the closed-loop system must adhere to $|v(t)|<V_S$ for most t and must have closed-loop dynamics that evolve much more slowly than the switching frequency.
3. We show how the objective of energy harvesting can be balanced against structural control objectives. Here, this is illustrated by requiring that the harvesting circuit be operated in such a way that the fraction of critical damping for all closed-loop system modes be above some threshold. This provides a generalization of many prior studies that have examined the interesting conflict between energy harvesting and structural damping objectives (Lesieutre et al., 2004; Liang and Liao, 2009; Shu and Lien, 2006). However, the technique we propose here is applicable to many other conflicting structural control objectives besides supplemental damping, such as disturbance rejection, tracking, and robustness objectives.
4. We illustrate how all the above issues can be handled in a unified way, through the use of linear matrix inequality (LMI)-based convex optimization techniques (Boyd et al., 1994). This is advantageous because once an optimization has been framed as an LMI problem, efficient interior point or primal-dual algorithms exist (and are widely available) to solve them.

Our discussion in this article is purely analytical; the goals are merely to provide a control theoretic framework for thinking about stochastic energy harvesting and for balancing energy harvesting against other response objectives. Considerable effort would be necessary to develop a practical H-bridge drive that can operate near the theoretical limits of its efficiency, as derived here. However, we see these issues as being beyond the scope of the article, which merely provides a theoretical motivation for such experimental investigations.

Energy harvesting as a feedback problem

Irrespective of what type of power conditioning circuit is used in an energy harvesting application, or how many transducers or disturbances are considered, one can characterize the system model by the block diagram shown in Figure 3. The block labeled "harvester" is the system illustrated in Figure 1, with inputs of a and i. The outputs of the harvester are voltage vector v, and also a vector z of other system response quantities deemed important. The electronics that condition and regulate the power extracted from the harvester may be characterized, for all practical purposes, by the following two quantities:

1. A feedback law K that maps present and past values of v into i. In some harvesting systems, additional feedback signals besides v (such as the harvester displacement in the SSHI circuit) also play a part in the feedback law for i. Note that the presence of feedback does not necessarily imply active control. Rather, it merely reflects the influence of the electronics on the harvester dynamics. Indeed, all the circuits in Figure 2 impose an associated feedback law K on the harvester dynamics.
2. A transmission loss model μ, which determines the power dissipation $P_{loss}(t)$ in the harvesting circuit, as a function of $v(\tau)$ and $i(\tau)$, for $\tau \leqslant t$. Clearly, $P_{loss}(t)$ may also depend on internal states of the circuit (which, in turn depend on present and past values of v and i, but also on the bus voltage V_S, switching states, etc.) and will in general be further parametrized by the specific hardware used to realize the circuit.

The power generated from the harvester at time t is

$$P_{gen}(t) = -i^T(t)v(t) - \mu(t) \tag{1}$$

In addition to the objective of optimizing generated power, we presume the response quantities in vector z (such as stresses, strains, voltage levels, accelerations, and current magnitudes) to be of importance. The power generation in stationary stochastic response is

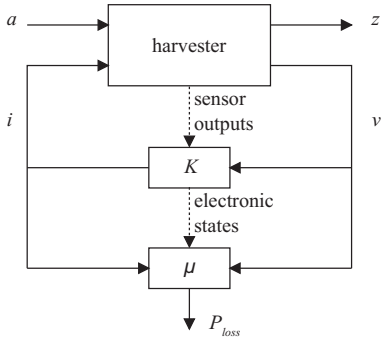

Figure 3. Block diagram of general energy harvesting problem.

$$\bar{P}_{gen} \triangleq \mathcal{E}\{-i^T v - \mu\} \tag{2}$$

Likewise, the stationary variances for each of the components of z is

$$\bar{s}_{zk} \triangleq \mathcal{E} z_k^2, \quad k = 1 \ldots n_z \tag{3}$$

We can then view the optimization of energy harvesting systems, both in terms of hardware parameters and intelligent control if it applies to a specific problem, as a constrained optimization. We have defined multiple objectives, one of which is the power generation in stationary response. We wish to optimize one of these objectives, subject to constraints on the others. In this analysis, we will narrow the focus to the specific problem of optimizing K to maximize $\bar{P}_{gen}$ subject to constraints on $\bar{s}_{zk}$, for a parametrized loss model μ. We will also place other constraints on the dynamic behavior of the closed-loop system in Figure 3.

In this context, the assumption that the currents are actively controlled by the H-bridge in Figure 2(e) simplifies the analysis, because it allows us to assume K can be chosen arbitrarily, that is, that it is not constrained to the highly specific dynamics of, for example, an SSHI circuit. It also allows us to design K to be a linear time-invariant feedback function of v, which makes the optimization tractable. However, the analysis does address the more complicated power dissipation associated with the control, in the sense that we will develop a detailed model for μ, and K will be optimized subject to this model.

The simplest modeling assumption we can make is that P_{loss} represents resistive (i.e. "i^2R") losses associated with power transmission, in which case we would say that $P_{loss} = i^T R i$, where $R > 0$ is a matrix characterizing the resistivity of the network. In this article, we consider more general models for P_{loss}, which merely retain the assumption that the dissipation may be expressed as a static function of i, that is

$$P_{loss} = \mu(i) \tag{4}$$

where $\mu(\cdot)$ may be nonquadratic, but is assumed to be time-invariant and positive-definite. In "Nonquadratic loss model of an H-bridge," we provide justification that these modeling assumptions are reasonable for H-bridge circuits. In the theory proposed in this article, we first introduce an analysis for quadratic μ and then *extend* this analysis to a class of generalized nonquadratic loss models as in equation (4).

Statement of the multi-objective optimal control problem

We presume a generic linear state space for the harvester of the form

$$\dot{x}_h = A_h x_h + B_{hi} i + B_{ha} a \tag{5a}$$

$$v = B_{hi}^T x_h \tag{5b}$$

$$z = C_h x_h + D_{hi} i + D_{ha} a \tag{5c}$$

where x_h is the system state vector. Assuming the energy harvester is a positive-real linear system (i.e. assuming it has no internal energy sources), the above mathematical characterization, with its dual use of the matrix B_{hi}, can be asserted without loss of generality (Brogliato et al., 2007).

We assume a is a stationary stochastic process with a rational, strictly proper power spectrum. In this case, it can be modeled as white noise, sent through a finite-dimensional filter, that is

$$\dot{x}_a = A_a x_a + B_a w \tag{6a}$$

$$a = C_a x_a \tag{6b}$$

where w is a white noise process with spectral intensity matrix $S_w = I$. Augmenting the control and disturbance states, the composite system state $x = [\,x_h^T \quad x_a^T\,]^T \in \mathbb{R}^n$ obeys

$$\dot{x} = Ax + B_i i + B_w w \tag{7a}$$

$$v = B_i^T x \tag{7b}$$

$$z = Cx + Di \tag{7c}$$

with appropriate definitions for the above-mentioned parameter matrices $\{A, B_i, B_w, C, D\}$.

We assume that the electronics are actively controlled via voltage feedback. Specifically, we assume a linear feedback controller $K(s) : v(s) \rightarrow i(s)$, where $K(s)$ is to be designed. We assume the order of $K(s)$ to be n (i.e. the same as that of the system model), and that $K(s)$ must be strictly proper. This implies a controller state space $\xi \in R^n$ characterized by

$$\dot{\xi} = A_K \xi + B_K v \tag{8a}$$

$$i = C_K \xi \tag{8b}$$

Augmenting the system states with the control states, the augmented state space $\chi = [\,x^T \quad \xi^T\,]^T$ is

$$\dot{\chi} = \mathcal{A}\chi + \mathcal{B} w \tag{9a}$$

$$v = \mathcal{C}_v \chi \tag{9b}$$

$$i = \mathcal{C}_i \chi \tag{9c}$$

$$z = \mathcal{C}_z \chi \tag{9d}$$

where

$$\mathcal{A} = \begin{bmatrix} A & B_i C_K \\ B_K B_i^T & A_K \end{bmatrix} \quad \mathcal{B} = \begin{bmatrix} B_w \\ 0 \end{bmatrix}$$

$$\mathcal{C}_v = [\,B_i^T \quad 0\,]$$

$$\mathcal{C}_i = [\,0 \quad C_K\,]$$

$$\mathcal{C}_z = [\,C \quad DC_K\,]$$

We wish to optimize $\{A_K, B_K, C_K\}$ to maximize $\bar{P}_{gen}$, subject to constraints on the response variances $\bar{s}_{zk}$. Without loss of generality, we assume that each response quantity z_k is normalized such that if $\bar{s}_{zk} = \bar{s}_{z\ell}$, this implies that responses z_k and z_ℓ are of equivalent acceptability. Thus, we can state the response constraint as $\bar{s}_{zk} < \gamma$, $k \in \{1 \ldots n_z\}$. In addition to these constraints, we will also require that the poles of the closed-loop system (i.e. the eigenvalues of $\mathcal{A}$) are in some region $\mathcal{M}$ in the s-plane. Specifically, we will define $\mathcal{M}$ as the region of eigenvalues with moduli less than a threshold ω_0 and damping ratios greater than a threshold ζ_0, that is

$$\mathcal{M} = \left\{ \lambda : |\lambda| < \omega_0,\ -\tfrac{\lambda + \bar{\lambda}}{2|\lambda|} > \zeta_0 \right\} \tag{10}$$

To summarize, we state the following multi-objective optimization problem, which will be denoted as Optimization Problem 1 ($OP1$)

$$OP1 : \begin{cases} \text{Maximize :} & \bar{P}_{gen} \\ \text{Over :} & A_K, B_K, C_K \\ \text{Constraints :} & \bar{s}_{zk} < \gamma : k = 1 \ldots n_z \\ & \text{spec}(\mathcal{A}) \subset \mathcal{M} \end{cases}$$

where $\text{spec}(\cdot)$ is the spectrum (i.e. set of eigenvalues) of $\mathcal{A}$.

Optimal control with resistive transmission loss model

In this section, we will develop the theory for how to solve $OP1$ when the loss model is resistive, that is,

$$\mu(i) = i^T R i \tag{11}$$

for some $R > 0$. This will be followed later in the article by an extension of the methods to a broader class of (more realistic) loss models.

Matrix inequality interpretation

Our first step is to recast each of the objectives and constraints from $OP1$ as an associated LMI. We begin by noting that $\mathcal{E}\chi\chi^T < S$ if and only if $S > 0$ and

$$\mathcal{A}S + S\mathcal{A}^T + \mathcal{B}\mathcal{B}^T < 0 \tag{12}$$

It follows that a given constraint $\bar{s}_{zk} < \gamma$ if and only if $\exists S_k = S_k^T > 0$ satisfying (12) as well as

$$\gamma > \mathcal{C}_{zk} S_k \mathcal{C}_{zk}^T \tag{13}$$

where $\mathcal{C}_{zk}$ is the kth row of $\mathcal{C}_z$. Equivalently, $\bar{s}_{zk} < \gamma$ if and only if $\exists P_k = P_k^T > 0$ satisfying

$$\begin{bmatrix} \mathcal{A}^T P_k + P_k \mathcal{A} & P_k \mathcal{B} \\ \mathcal{B}^T P_k & -I \end{bmatrix} < 0 \tag{14}$$

$$\begin{bmatrix} \gamma & \mathcal{C}_{zk} \\ \mathcal{C}_{zk}^T & P_k \end{bmatrix} > 0 \tag{15}$$

To put the optimization of $\bar{P}_{gen}$ in terms of matrix inequalities, we invoke a result proved in Scruggs (2010), which states that for any stabilizing feedback law $K(s)$, $\bar{P}_{gen}$ may be expressed as

$$\bar{P}_{gen} = \bar{P}_{gen}^{max} - \mathcal{E}\|i - Fx\|_R^2 \tag{16}$$

where

$$\bar{P}_{gen}^{max} = -\tfrac{1}{2} tr\left\{ B_w^T Q B_w \right\} \tag{17}$$

$$F = -\tfrac{1}{2} R^{-1} B_i^T [Q + I] \tag{18}$$

and Q is the solution to the nonstandard Riccati equation

$$0 = A^T Q + QA - \tfrac{1}{2}[Q + I] B_i R^{-1} B_i^T [Q + I] \tag{19}$$

(In Scruggs (2010), it is proved that this equation has a solution if the transfer function from i to v is positive real in the weakly strict sense. Speaking loosely, this implies that the harvester is asymptotically stable and the driving point impedance of the harvester is passive.) Note that $\bar{P}_{gen}^{max}$ is algebraically related to the system parameters, but does not depend on the way the current i is controlled. The maximization of $\bar{P}_{gen}$ is therefore equivalent to the minimization of its departure from the feedback-invariant upper bound $\bar{P}_{gen}^{max}$, that is, the minimization of $\mathcal{E}\|i - Fx\|_R^2$.

As such, for some $\theta \in R$, we have that $\bar{P}_{gen} > \theta$ if and only if $\exists S_P > 0$ satisfying (12) together with

$$\text{tr}\left\{ R(\mathcal{C}_i - \mathcal{F}) S_P (\mathcal{C}_i - \mathcal{F})^T \right\} - \bar{P}_{gen}^{max} + \theta < 0 \tag{20}$$

where

$$\mathcal{F} = [F \quad 0] \tag{21}$$

An equivalent condition is that $\exists P_P > 0$ and $W = W^T$ such that

$$\begin{bmatrix} \mathcal{A}^T P_P + P_P \mathcal{A} & P_P \mathcal{B} \\ \mathcal{B}^T P_P & -I \end{bmatrix} < 0 \tag{22}$$

$$\begin{bmatrix} W & \mathcal{C}_i - \mathcal{F} \\ \mathcal{C}_i^T - \mathcal{F}^T & P_P \end{bmatrix} > 0 \tag{23}$$

$$\text{tr}\{RW\} - \bar{P}_{gen}^{max} + \theta < 0 \tag{24}$$

We note that with no introduction of conservatism, we may set the equivalency

$$P_P = P_1 = \ldots = P_{n_z} \tag{25}$$

To see this, consider that for any $\{\theta, \gamma\}$ resulting in a feasible solution to LMIs (14), (15), (22), (23), and (24),

the region of feasibility is maximized by setting $P_P = P_k = S_\varepsilon^{-1}$ where S_ε is the solution to

$$\mathcal{A}S_\varepsilon + S_\varepsilon\mathcal{A}^T + \mathcal{B}\mathcal{B}^T + \varepsilon I = 0 \tag{26}$$

for $\varepsilon \to 0$. Thus, we have that $\bar{s}_{zk} < \gamma$, $k \in \{1 \ldots n_z\}$ and $\bar{P}_{gen} < \theta$ if and only if $\exists P > 0$ and $W = W^T$ such that (24) holds, together with

$$\begin{bmatrix} \mathcal{A}^T P + P\mathcal{A} & P\mathcal{B} \\ \mathcal{B}^T P & -I \end{bmatrix} < 0 \tag{27}$$

$$\begin{bmatrix} \gamma & \mathcal{C}_{zk} \\ \mathcal{C}_{zk}^T & P \end{bmatrix} > 0 \tag{28}$$

$$\begin{bmatrix} W & \mathcal{C}_i - \mathcal{F} \\ \mathcal{C}_i^T - \mathcal{F}^T & P \end{bmatrix} > 0 \tag{29}$$

Now, we turn our attention to the pole placement constraint. First, we note that for any stable matrix $\mathcal{A}$, the region $\mathcal{M}$ in the open left-half plane (denoted C^-), as characterized by equation (10), may be restated as

$$\mathcal{M} = \left\{ s \in C^- : L_k + sM_k + \bar{s}M_k^T < 0, \quad k \in \{\omega, \zeta\} \right\} \tag{30}$$

where

$$L_\omega = -\omega_0 I_2 \quad M_\omega = \begin{bmatrix} 0 & 1 \\ 0 & 0 \end{bmatrix} \tag{31}$$

$$L_\zeta = 0_{2\times 2} \quad M_\zeta = \begin{bmatrix} 1 & \alpha \\ -\alpha & 1 \end{bmatrix} \tag{32}$$

where $\alpha = \zeta_0 / \sqrt{1 - \zeta_0^2}$. We then have that as proved in Chilali and Gahinet (1996), an asymptotically stable $\mathcal{A}$ has its eigenvalues in $\mathcal{M}$ if and only if $\exists P_\omega > 0$, $P_\zeta > 0$ such that

$$L_k \otimes P_k + M_k \otimes \left(\mathcal{A}^T P_k\right) + \left(M_k^T\right) \otimes \left(P_k \mathcal{A}\right) < 0, \quad k \in \{\omega, \zeta\} \tag{33}$$

where " $\otimes$ " denotes the Kronecker product.

We now impose the conservative restriction that

$$P_\omega = P_\zeta = P \tag{34}$$

In so doing, we can append the LMIs

$$\begin{bmatrix} -\omega_0 P & \mathcal{A}^T P \\ P\mathcal{A} & -\omega_0 P \end{bmatrix} < 0 \tag{35}$$

$$\begin{bmatrix} \mathcal{A}^T P + P\mathcal{A} & \alpha\left(\mathcal{A}^T P - P\mathcal{A}\right) \\ \alpha\left(P\mathcal{A} - \mathcal{A}^T P\right) & \mathcal{A}^T P + P\mathcal{A} \end{bmatrix} < 0 \tag{36}$$

to the previous set of LMIs (24) and (27) to (29), to form the full feasibility set for the multi-objective feedback design problem. We emphasize that up until the imposition of equation (34), no conservatism had been introduced into the feasibility criteria. Equating the various Lyapunov matrices as in equation (34) is called "Lyapunov shaping" and is a conservative assumption imposed in order to arrive at a convex optimization problem.

Convex design problem

With the matrix inequalities from the previous section defined, we now use standard LMI techniques, as outlined by Scherer et al. (1997), to arrive at a convex semi-definite program. To summarize the standard results, we partition P and its inverse as

$$P = \begin{bmatrix} Y & N \\ N^T & \bullet \end{bmatrix} \qquad P^{-1} = \begin{bmatrix} X & M \\ M^T & \bullet \end{bmatrix} \tag{37}$$

where $\bullet$ implies a matrix sub-block that does not need to be known, and where $X = X^T$ and $Y = Y^T$. Next, define the transformation matrix

$$\Pi_1 = \begin{bmatrix} X & I \\ M^T & 0 \end{bmatrix} \tag{38}$$

and note that the following transformations occur

$$\Pi_1^T P \mathcal{A} \Pi_1 = \begin{bmatrix} AX + B_i\hat{C} & A \\ \hat{A} & YA + \hat{B}B_i^T \end{bmatrix} \tag{39}$$

$$\Pi_1^T P \mathcal{B} = \begin{bmatrix} B_w \\ YB_w \end{bmatrix} \tag{40}$$

$$\mathcal{C}_v \Pi_1 = \begin{bmatrix} B_i^T X & B_i^T \end{bmatrix} \tag{41}$$

$$\mathcal{C}_i \Pi_1 = \begin{bmatrix} \hat{C} & 0 \end{bmatrix} \tag{42}$$

$$\mathcal{C}_z \Pi_1 = \begin{bmatrix} CX + D\hat{C} & C \end{bmatrix} \tag{43}$$

$$\mathcal{F} \Pi_1 = \begin{bmatrix} FX & F \end{bmatrix} \tag{44}$$

$$\Pi_1^T P \Pi_1 = \begin{bmatrix} X & I \\ I & Y \end{bmatrix} \tag{45}$$

where the variables

$$\hat{A} = NA_K M^T + NB_K B_i^T X + YB_i C_K M^T + YAX \tag{46a}$$

$$\hat{B} = NB_K \tag{46b}$$

$$\hat{C} = C_K M^T \tag{46c}$$

become the transformed control design variables. The reason for performing these transformations is that they permit LMIs (27) to (29), (35), and (36) to become linear in the variables $\{X, Y, \hat{A}, \hat{B}, \hat{C}, W, \gamma, \theta\}$. Specifically, they respectively become

$$\begin{bmatrix} \Delta_1 + \Delta_1^T & A + \hat{A}^T & B_w \\ & \Delta_2 + \Delta_2^T & YB_w \\ (\text{sym}) & & -I \end{bmatrix} < 0 \tag{47}$$

$$\begin{bmatrix} -\gamma & C_kX + D_k\hat{C} & C_k \\ & -X & -I \\ (\text{sym}) & & -Y \end{bmatrix} < 0 \tag{48}$$

$$\begin{bmatrix} W & \hat{C} - FX & -F \\ & X & I \\ (\text{sym}) & & Y \end{bmatrix} > 0 \tag{49}$$

$$\begin{bmatrix} -\omega_0 X & -\omega_0 I & \Delta_1^T & \hat{A}^T \\ & -\omega_0 Y & A^T & \Delta_2^T \\ & & -\omega_0 X & -\omega_0 I \\ (\text{sym}) & & & -\omega_0 Y \end{bmatrix} < 0 \tag{50}$$

$$\begin{bmatrix} \Delta_1 + \Delta_1^T & A + \hat{A}^T & \alpha\left(\Delta_1^T - \Delta_1\right) & \alpha\left(\hat{A}^T - A\right) \\ & \Delta_2 + \Delta_2^T & \alpha\left(A^T - \hat{A}\right) & \alpha\left(\Delta_2^T - \Delta_2\right) \\ & & \Delta_1 + \Delta_1^T & A + \hat{A}^T \\ (\text{sym}) & & & \Delta_2 + \Delta_2^T \end{bmatrix} < 0 \tag{51}$$

where

$$\Delta_1 = AX + B_i\hat{C} \tag{52}$$

$$\Delta_2 = YA + \hat{B}B_i^T \tag{53}$$

With the problem transformed as such, the following optimization is a standard (convex) LMI eigenvalue problem, which we will call *OP*2

$$OP2: \begin{cases} \text{Maximize :} & \bar{P}_{gen}^{\max} - \text{tr}\{RW\} \\ \text{Over :} & \{X, Y, \hat{A}, \hat{B}, \hat{C}, W\} \\ \text{Constraints :} & (47), (48), (49), (50), (51) \end{cases}$$

Let the optimal solution be $\{X^\star, Y^\star, \hat{A}^\star, \hat{B}^\star, \hat{C}^\star, W^\star\}$. Then, because *OP*2 is always more conservative than *OP*1, we have that the resultant power generation $\bar{P}_{gen}^\star$ at the optimum is under-bounded by the maximization objective, that is,

$$\bar{P}_{gen}^\star \geq \bar{P}_{gen}^{max} - \text{tr}\{RW^\star\} \tag{54}$$

To obtain a set of controller state space parameters $\{A_K, B_K, C_K\}$ that achieve the optimized performance bound in equation (54), we first find M and N. An infinite number of equivalent realizations exist, and consequently, there will be an infinite number of valid $\{M, N\}$ combinations. It is only important that they bring about the inverse relations in equation (37), which is ensured by

$$X^\star Y^\star + MN^T = I \tag{55}$$

Thus, with $\{X^\star, Y^\star\}$ solved, we may find a valid pair $\{M, N\}$ by performing the singular value decomposition

$$U\Sigma V^T = I - X^\star Y^\star \tag{56}$$

where Σ is diagonal and positive semidefinite, and $\{U, V\}$ are unitary. Then, one can find

$$M = U\Sigma^{1/2} \quad N = V\Sigma^{1/2} \tag{57}$$

With these solved, we can then find the inverse mapping of equation (46) as

$$C_K = \hat{C}^\star M^{-T} \tag{58a}$$

$$B_K = N^{-1}\hat{B}^\star \tag{58b}$$

$$A_K = N^{-1}\left(\hat{A}^\star - Y^\star AX^\star - Y^\star B_i\hat{C}^\star - \hat{B}^\star B_i^T X^\star\right)M^{-T} \tag{58c}$$

With the control parameters known, we may find the actual (i.e. nonconservative) value of $\bar{P}_{gen}^\star$ achieved by the optimized controller by solving the closed-loop covariance matrix via the Lyapunov equation

$$\mathcal{A}S^\star + S^\star\mathcal{A}^T + \mathcal{B}\mathcal{B}^T = 0 \tag{59}$$

with the optimal $\{A_K, B_K, C_K\}$ parameters inserted into $\mathcal{A}$ and $\mathcal{B}$, and then evaluating

$$\bar{P}_{gen}^\star = \bar{P}_{gen}^{max} - tr\left\{R(\mathcal{C}_i - \mathcal{F})S^\star(\mathcal{C}_i - \mathcal{F})^T\right\} \tag{60}$$

Similarly, the actual (nonconservative) values of $\bar{s}_{zk}^\star$ are each $\mathcal{C}_{zk}S^\star\mathcal{C}_{zk}^T$.

Note that although we have framed this problem with $\bar{P}_{gen}$ as the target for optimization, subject to the constraints that $\bar{s}_{zk} < \gamma$ together with the regional constraint on the poles, we could have just as easily optimized the bound γ for the $\bar{s}_{zk}$ values (or the shape of pole placement region $\mathcal{M}$, for that matter) subject to the constraint $\bar{P}_{gen} > \theta$, for some specified θ. Doing this modifies the optimization only superficially—all the LMIs remain the same, although equation (24) would have to be imposed explicitly as a constraint in *OP*2 for this case, whereas in the optimization of $\bar{P}_{gen}$, its imposition was unnecessary. Additionally, if $n_z > 1$, the variable γ would become a free optimization variable in the design space, with its value being the minimization objective.

Nonquadratic loss models

Nonquadratic loss model of an H-bridge

Consider again the H-bridge in Figure 2(e). In this circuit, each MOSFET/diode pair is operated like a power-electronic switch. In this article, we consider the operation of this system in bidirectional discontinuous conduction mode. In this operation regime, a given transducer's current is controlled to take on the shape shown in Figure 4. As shown, current from the transducer is controlled in triangular bursts, which are triggered by a switching clock with period t_s. The switching

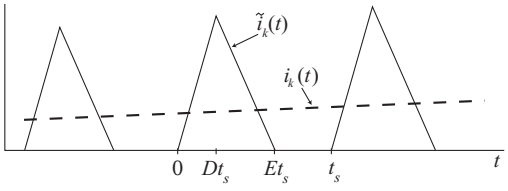

Figure 4. Current of transducer k in discontinuous conduction: actual current $\tilde{i}_k$ and low-frequency component (i.e. average-switched value) i_k.

frequency $f_s = 1/t_s$ is presumed to be at least a decade above the predominant dynamics of the harvester (i.e. $\frac{1}{2\pi}\omega_0$), and as such, the high-frequency component of the current is assumed to be filtered by the transducer capacitance. Consequently, it is only the low-frequency switch-averaged current that significantly influences the overall system response. For clarity, we refer to i_k as the low-frequency average-switched signal, and $\tilde{i}_k$ as the actual current with its high-frequency content included.

For the analysis of the H-bridge, we will drop the transducer number subscript k, to simplify the notation. At the beginning of the given switching cycle (i.e. $t = 0$), $\tilde{i}(0) = 0$. Depending on whether the desired average current is positive or negative, either MOSFETs 1 and 4, or MOSFETs 2 and 3 (respectively) are switched on at $t = 0$. Assuming the storage voltage V_S is greater than the magnitude $|v|$ of the transducer voltage, this will cause current to flow through the transducer and inductor. The MOSFETs remain switched on over the period $t \in [0, Dt_s]$, where D is the controllable duty cycle. During this time, the differential equation for the evolution of current magnitude $|\tilde{i}|$ is

$$L\tfrac{d}{dt}|\tilde{i}| = V_S - v\,\mathrm{sgn}(\tilde{i}) - V_1(\tilde{i}) \tag{61}$$

where $V_1(\cdot)$ is the (possibly) nonlinear conduction voltage of the conducting path of the H-bridge, including the MOSFETs as well as possibly the series resistance of the transducer and inductor. We will assume it to be an affine function of $|\tilde{i}|$

$$V_1 = V_{01} + R_1|\tilde{i}| \tag{62}$$

that is, energy is dissipated like a diode in series with a resistor. At time $t = Dt_s$, we have that

$$|\tilde{i}(Dt_s)| = \frac{V_S - v\,\mathrm{sgn}(\tilde{i}) - V_{01}}{R_1}\left(1 - e^{-R_1 Dt_s/L}\right) \tag{63}$$

Assuming $Dt_s R_1/L \ll 1$, this is approximately

$$|\tilde{i}(Dt_s)| = \frac{V_S - v\,\mathrm{sgn}(\tilde{i}) - V_{01}}{L} Dt_s \tag{64}$$

At this time, the MOSFETs are switched off. The presence of the inductance in the conductive path then triggers the free-wheeling diodes to conduct, causing the inductor to demagnetize, arriving at $|\tilde{i}| = 0$ at time $t = Et_s$. During the demagnetizing time $t \in [Dt_s, Et_s]$, the differential equation for $|\tilde{i}|$ is

$$L\tfrac{d}{dt}|\tilde{i}| = -V_S - v\,\mathrm{sgn}(\tilde{i}) - V_2(\tilde{i}) \tag{65}$$

where $V_2(\cdot)$, defined similarly to $V_1(\cdot)$, is the switch conduction voltage, which we assume similarly to be

$$V_2 = V_{02} + R_2|\tilde{i}| \tag{66}$$

However, note that because the current is routed through diodes instead of MOSFETs in the demagnetizing phase, it will be the case that $V_{01} \neq V_{02}$ and $R_{01} \neq R_{02}$. Using a similar reasoning to that for the magnetizing phase, $|\tilde{i}(Dt_s)|$ is derived in terms of E as

$$|\tilde{i}(Dt_s)| = \frac{V_S + v\,\mathrm{sgn}(\tilde{i}) + V_{02}}{L}(E - D)t_s \tag{67}$$

Thus, equating equation (64) with equation (67) gives

$$\frac{E - D}{D} = \frac{V_S - v\,\mathrm{sgn}(\tilde{i}) - V_{01}}{V_S + v\,\mathrm{sgn}(\tilde{i}) + V_{02}} \tag{68}$$

As discussed, it is generally true that $R_1 \neq R_2$ and $V_{01} \neq V_{02}$. However, we can simplify the math by assuming that each switch exhibits the conductive dissipation which involves the maximum of each of these parameters, in both the magnetizing and demagnetizing phases. Thus, we make the conservative substitution

$$V_{01}, V_{02} \leftarrow V_0 \triangleq \max\{V_{01}, V_{02}\} \tag{69}$$

$$R_1, R_2 \leftarrow R_0 \triangleq \max\{R_1, R_2\} \tag{70}$$

We emphasize that although this results in a simplification of the system loss model, it is always *conservative*, in the sense that it will result in an overestimation of the system losses.

So doing, the two key quantities we will need for our analysis become

$$|\tilde{i}(Dt_s)| = \frac{V_S - v\,\mathrm{sgn}(\tilde{i}) - V_0}{L} Dt_s \tag{71}$$

and

$$\frac{E - D}{D} = \frac{V_S - v\,\mathrm{sgn}(\tilde{i}) - V_0}{V_S + v\,\mathrm{sgn}(\tilde{i}) + V_0} \tag{72}$$

From equation (72), we have that

$$E = \frac{2V_S}{V_S + v\,\mathrm{sgn}(\tilde{i}) + V_0} D \tag{73}$$

Denote $\text{avg}_{[0,\,t_s]}|\tilde{i}|$ as the average current magnitude over the switching cycle. From the geometry of the triangular waveform, we have that

$$\text{avg}_{[0,\,t_s]}|\tilde{i}| = \frac{E|\tilde{i}(Dt_s)|}{2} \tag{74}$$

$$= \frac{V_S}{f_s L}\frac{V_S - v\,\text{sgn}(\tilde{i}) - V_0}{V_S + v\,\text{sgn}(\tilde{i}) + V_0}D^2 \tag{75}$$

As such, for switching cycle N with $t \in [Nt_s, (N+1)t_s]$, the low-frequency component of $\tilde{i}$ can be controlled via D, that is,

$$|i(t)| \approx \text{avg}_{[Nt_s,\,(N+1)t_s]}|\tilde{i}| \quad , \quad t \in [Nt_s, (N+1)t_s] \tag{76}$$

with the sign of i during this interval being determined by triggering the proper combination of MOSFETs.

Using the above equations and again resorting to the geometry of the triangular waveform, we next find the average value of $\tilde{i}^2$. Suppressing the details, we simply note that it can be expressed as

$$\text{avg}_{[0,\,t_s]}\tilde{i}^2 = \frac{2}{3}\sqrt{\frac{V_S^2 - \left(v\,\text{sgn}(\tilde{i}) + V_0\right)^2}{f_s L V_S}}\left\{\text{avg}_{[0,\,t_s]}|\tilde{i}|\right\}^{\frac{3}{2}} \tag{77}$$

which can be conservatively approximated as

$$\text{avg}_{[0,\,t_s]}\tilde{i}^2 = \frac{2}{3}\sqrt{\frac{V_S}{f_s L}}\left\{\text{avg}_{[0,\,t_s]}|\tilde{i}|\right\}^{\frac{3}{2}} \tag{78}$$

Now, the conductive losses incurred in one switching cycle may be expressed as

$$\mu_c = \text{avg}_{[0,\,t_s]}\left\{V_0|\tilde{i}| + R_0\tilde{i}^2\right\} \tag{79}$$

$$= V_0\,\text{avg}_{[0,\,t_s]}|\tilde{i}| + R_0\frac{2}{3}\sqrt{\frac{V_S}{f_s L}}\left\{\text{avg}_{[0,\,t_s]}|\tilde{i}|\right\}^{\frac{3}{2}} \tag{80}$$

thus, in light of equation (76)

$$\mu_c(i) = V_0|i| + R_0\frac{2}{3}\sqrt{\frac{V_S}{f_s L}}|i|^{\frac{3}{2}} \tag{81}$$

We can add more detail to this loss model by also including gating and transition losses, denoted μ_g and μ_t. Gating losses constitute a certain amount of energy U_g expended every time the MOSFETs are switched on. As such, the average power dissipated in gating is

$$\mu_g = U_g f_s \tag{82}$$

Transition losses constitute dissipation as the MOSFETs transition from being on to off. Assuming a linear load line for the voltage–current relationship for the switches, we have that the energy dissipated for a single MOSFET during a transition is approximately $V_S|\tilde{i}(Dt_s)|\tau_t$, where τ_t is the transition time. We may find $|\tilde{i}(Dt_s)|$ in terms of $\text{avg}_{[0,\,t_s]}|\tilde{i}|$ as

$$|\tilde{i}(Dt_s)| = \sqrt{\frac{V_S^2 - \left(v\,\text{sgn}(\tilde{i}) + V_0\right)^2}{f_s L V_S}\,\text{avg}_{[0,\,t_s]}|\tilde{i}|} \tag{83}$$

which may be conservatively approximated by

$$|\tilde{i}(Dt_s)| = \sqrt{\frac{V_S}{f_s L}}\left\{\text{avg}_{[0,\,t_s]}|\tilde{i}|\right\}^{\frac{1}{2}} \tag{84}$$

Thus, the total transition loss (for both MOSFETs) can be approximated as

$$\mu_t(i) = 2\sqrt{\frac{V_S}{f_s L}}V_S\tau_t|i|^{\frac{1}{2}} \tag{85}$$

Adding μ_g and μ_t to equation (81), we arrive at

$$\mu(i) = U_g f_s + 2\sqrt{\frac{V_S}{f_s L}}V_S\tau_t|i|^{\frac{1}{2}} + V_0|i| + R_0\frac{2}{3}\sqrt{\frac{V_S}{f_s L}}|i|^{\frac{3}{2}} \tag{86}$$

It thus follows that the total loss model for a multi-transducer system is just the summation of $\mu_k(i_k)$, $k = 1 \ldots n_p$, with each found as above.

Note that many conservative approximations were made, by which we arrived at this model. If the bounding approximations (77) → (78) and (83) → (84) were not made, then μ would depend on v as well as i. Additionally, if we did not introduce the conservative substitutions (69) and (70), the mathematics would have been considerably more elaborate. However, these more accurate models would complicate the ensuing analysis, and we will therefore retain the conservatism.

Operational constraints on voltage and current

In the development above, assumptions were made regarding the magnitudes of i and v, which are necessary for discontinuous conduction to be possible. First, it must be the case that

$$|v| < V_S \tag{87}$$

in order for the drive to operate properly. If this condition is violated, two-way power conversion ceases to be possible, because the MOSFETs will not be forward biased when gated. In this article, we address constraint (87) explicitly by suppressing v as a competing objective to the energy harvesting objective, such that (87) holds most of the time. This can be done by including v in the performance vector z and enforcing the condition

$$\mathcal{E}v^2 \leqslant (V_S/\delta)^2 \tag{88}$$

that is, we require that the stationary probability distribution for v be such that it contains at least δ standard

deviations in the range $|v|<V_S$. For δ sufficiently large, this ensures that most of the time, the transducer voltages are below the bus voltage. In general, a δ value at or above 2 should be used.

Additionally, in order for the system to be in discontinuous conduction, $E<1$ is necessary. This implies that the value of i is restricted as well. From equations (73) and (75), and again assuming equation (76) we have that

$$E^2 = \frac{4V_S f_s L}{V_S^2 - (v\,\mathrm{sgn}(i) + V_0)^2}|i| \tag{89}$$

from which we conclude that i is restricted to

$$|i| < \frac{V_S^2 - (v\,\mathrm{sgn}(i) + V_0)^2}{4V_S f_s L} \tag{90}$$

If this condition is violated, electronics must be operated in continuous conduction in order to realize current i. This does not present any problems, except that the loss model we have derived is different from that of the continuous conduction case.

In addition to the above constraint, another limitation on i arises from the assumptions $Dt_s R_0/L \ll 1$ and $(E-D)t_s R_0/L \ll 1$, which are what justify the triangular discontinuous conduction waveform in Figure 4. Using equations (75) and (73), we have that these constraints are, respectively

$$R_0\sqrt{\frac{i}{Lf_sV_S}}\sqrt{\frac{V_S + v\,\mathrm{sgn}(i) + V_0}{V_S - v\,\mathrm{sgn}(i) - V_0}} \ll 1 \tag{91}$$

$$R_0\sqrt{\frac{i}{Lf_sV_S}}\sqrt{\frac{V_S - v\,\mathrm{sgn}(i) - V_0}{V_S + v\,\mathrm{sgn}(i) + V_0}} \ll 1 \tag{92}$$

For the examples to be considered in this article, it was found that due to the hardware parameters used in the example, constraints (90), (91), and (92) did not need to be explicitly enforced for the problem, as they were found to hold anyway at the optimal solutions. However, if necessary they could be approximately enforced in a similar (albeit more complicated) reasoning leading to equation (88).

Extension of OP2 to accommodate nonquadratic loss models

We now propose a technique for expanding the theory of section "Optimal control with resistive transmission loss model" to accommodate nonquadratic loss functions. Although the algorithm proposed in this section could be applied to a broad class of loss models, to simplify the analysis we will presume $\mu(i)$ may be broken down into a component-wise summation of loss functions for each current i_k, separately, as in the case of the loss model derived above for the discontinuously conducting active drive, that is

$$\mu(i) = \sum_{k=1}^{n_p} \mu_k(i_k) \tag{93}$$

To begin, we presume that the electronics are still controlled to effect a linear closed-loop system, that is, we presume the feedback controller is still a linear feedback law $K(s) : v \to i$. It is important to emphasize that this assumption is imposed in order to make the analysis and optimization tractable. In general, depending on the loss model, there may be nonlinear controllers that outperform the best linear controller. However, such issues are beyond the scope of this article.

If the dynamics of the closed-loop system are linear, then the response distribution for the composite system state χ is Gaussian. Consequently, the distributions for each of the currents i_k is Gaussian, with zero mean and variance $\bar{s}_{ik} = \mathcal{E}i_k^2$. Then, we may evaluate the average loss for transducer k as

$$\mathcal{E}\mu_k = \frac{1}{\sqrt{2\pi\bar{s}_{ik}}}\int_{-\infty}^{\infty} e^{-i_k^2/2\bar{s}_{ik}}\mu_k(i_k)di_k \tag{94}$$

For example, for the loss model derived in the last section for an active drive in discontinuous conduction, we have that

$$\mathcal{E}\mu_k = U_g f_s + 2\left(V_S\tau_t\Gamma\left(\tfrac{3}{4}\right)\sqrt{\frac{2^{1/2}V_S}{\pi L f_s}}\right)\bar{s}_{ik}^{\frac{1}{4}} + \left(V_0\sqrt{\frac{2}{\pi}}\right)\bar{s}_{ik}^{1/2} + \left(\frac{2}{3}R_0\Gamma\left(\tfrac{7}{4}\right)\sqrt{\frac{2^{3/2}V_S}{\pi f_s L}}\right)\bar{s}_{ik}^{\frac{3}{4}} \tag{95}$$

where $\Gamma(z) \triangleq \int_0^\infty q^{z-1}e^{-q}dq$ is the standard gamma function.

Now, we make an important observation. If $\mathcal{E}\mu_k$ is semiconcave, that is, if

$$\frac{\partial^2\mathcal{E}\mu_k}{\partial\bar{s}_{ik}^2} \leqslant 0, \quad \forall\bar{s}_{ik} > 0 \tag{96}$$

then it follows that $\mathcal{E}\mu_k$ can be conservatively approximated (i.e. overbounded) by its first-order Taylor expansion about any positive variance $\bar{s}_{ik} = \bar{s}_{ik}^0$, that is,

$$\mathcal{E}\mu_k \leqslant \mu_k^0 + R_k^0\bar{s}_{ik} \tag{97}$$

where

$$R_k^0 = \left.\frac{\partial\mathcal{E}\mu_k}{\partial\bar{s}_{ik}}\right|_{\bar{s}_{ik}=\bar{s}_{ik}^0} \tag{98}$$

$$\mu_k^0 = \mathcal{E}\mu_k|_{\bar{s}_{ik}=\bar{s}_{ik}^0} - R_k^0\bar{s}_{ik}^0 \tag{99}$$

with the equality holding (as well as the slope) where $\bar{s}_{ik} = \bar{s}_{ik}^0$. For example, the loss model derived in the last section is semiconcave, due to the fact that all terms in equation (95) involve $\bar{s}_{ik}^c$ for $c \leqslant 1$.

So for semiconcave loss models, we may conservatively over-bound them by a summation of a static (i.e. current-independent) loss model and a quadratic (i.e. resistive) loss model. While it is certainly not the case that all loss models for all power conversion systems have the semiconcave property, it does appear to hold for a variety of power-electronic converter operating regimes such as the one under consideration in this article. The property is important because it permits us, without the introduction of any further conservatism, to nest our previous algorithm from section "Matrix inequality interpretation" to section "Convex design problem" for resistive losses, inside an iterative algorithm for nonquadratic losses. This algorithm, which executes what we will call Optimization Problem 3 (*OP*3), can be stated as follows

$$OP3: \begin{cases} \text{Step 0:} & \text{Take any arbitary values for } \bar{s}_{ik}^0 > 0, \\ & \text{and compute } R^0 \text{ via (98)} \\ \text{Step 1:} & \text{For } R \leftarrow R^0, \text{ find} \{X^\star, Y^\star, \hat{A}^\star, \hat{B}^\star \\ & \hat{C}^\star, W^\star\} \text{as in } OP2 \\ \text{Step 2:} & \text{For the optimized parameters, find the} \\ & \text{associated } S^\star, \text{ as in (59)} \\ \text{Step 3:} & \text{Find new values for the current} \\ & \text{variances, as } \bar{s}_{ik} = C_{ik} S^\star C_{ik} \\ \text{Step 4:} & \text{For the new values of } \bar{s}_{ik}, \text{ set } \bar{s}_k^0 \leftarrow \bar{s}_{ik}, \\ & \text{recompute } R^0 \text{ via (98), and return to step 1} \end{cases}$$

The semiconcavity property of $\mathcal{E}\mu_k$ implies that the above algorithm, upon execution, will result in monotonically increasing $\bar{P}_{gen}$ for each successive iteration of *OP*3. Because $\bar{P}_{gen}$ also has a physical upper bound that is independent of R (as derived in Scruggs (2009)), the algorithm is therefore guaranteed to converge.

As in section "Convex design problem," let the convergent solution have parameters $\{X^\star, Y^\star, \hat{A}^\star, \hat{B}^\star, \hat{C}^\star, W^\star\}$, and let the power generation at the optimal solution be $\bar{P}_{gen}^\star$. Then analogous to equation (54), this power generation is under-bounded by

$$\bar{P}_{gen}^\star \geq -\tfrac{1}{2} tr\{B_w^T Q B_w\} - \sum_{k=1}^{n_p} \mu_{ik}^0 - tr\{R^0 W^\star\} \quad (100)$$

where the expression on the right-hand side is the objective optimized by algorithm *OP*3, and where Q is the solution to Riccati equation (19) with $R \leftarrow R^0$. Also, analogously to equation (60), the actual value of $\bar{P}_{gen}^\star$ at the optimal solution is

$$\bar{P}_{gen}^\star = -\tfrac{1}{2} tr\{B_w^T Q B_w\} - \sum_{k=1}^{n_p} \mu_{ik}^0 - tr\left\{R^0 (\mathcal{C}_i - \mathcal{F}) S^\star (\mathcal{C}_i - \mathcal{F})^T\right\} \quad (101)$$

where $S^\star$ is the closed-loop covariance matrix at the optimum design and is the solution to equation (59).

Example: piezoelectric energy harvesting

The primary objective of this article thus far has been to propose a set of tools for the optimization of feedback in active energy harvesting circuits. We close the article with an example of a potential application of these concepts to piezoelectric energy harvesting. This example also illustrates how the more detailed loss model we have developed in the previous sections points toward concurrent optimal design of the feedback controller and the operating parameters (i.e. bus voltage and switching frequency) of the electronics.

In this example, we consider a single-transducer piezoelectric bimorph cantilever beam in which the fundamental vibratory mode dominates the system response. In this case, the harvester state space is $x_h = [\,q \quad \dot{q} \quad p\,]^T$, where q is the generalized mechanical displacement of the beam, and p is the generalized charge displacement. The differential equation has coefficients

$$A_h = \begin{bmatrix} 0 & \omega_1 & 0 \\ -\omega_1 & -2\zeta_1\omega_1 & \theta_1 \\ 0 & -\theta_1 & -1/\tau \end{bmatrix}, \; B_{hi} = \begin{bmatrix} 0 \\ 0 \\ \beta \end{bmatrix}, \; B_{ha} = \begin{bmatrix} 0 \\ \eta_1 \\ 0 \end{bmatrix} \quad (102)$$

In this example, we will take $z = v$, that is, our objective will be to maximize $\bar{P}_{gen}$ subject to a constraint on the variance of the transducer voltage. (Recall that this constraint is motivated by the need to control the transducer current.) Thus, we have $C = B_i^T$ and $D = 0$.

Specifically, we presume the data of this problem to be the same as that used in prior, similar studies, and ultimately derived from the parameters identified by Sodano et al. (2004). These are $\omega_1 = 241\,\text{rad/s}$, $\zeta_1 = 0.01$, $\theta_1 = 65.8\,\text{s}^{-1}$, $\eta_1 = 0.092\sqrt{\text{kg}}$, $\tau = 2\,\text{s}$, and $\beta = 1770\sqrt{\Omega/\text{s}}$.

For the disturbance, we presume the noise filter to be second-order filtered noise, characterized by the data

$$A_a = \begin{bmatrix} 0 & \omega_a \\ -\omega_a & -2\zeta_a\omega_a \end{bmatrix}, \quad B_a = C_a^T = \begin{bmatrix} 0 \\ (4\zeta_a\omega_a\sigma_a^2)^{1/4} \end{bmatrix} \quad (103)$$

This produces a stochastic process with an RMS value of σ_a, and with spectrum centered at the frequency ω_a with a quality factor governed by ζ_a. Specifically, we presume that $\omega_a = 249\,\text{rad/s}$, $\zeta_a = 0.2$, and for various values of σ_a.

For the loss model, we assume the parameters listed in Table 1 and justify them as follows. We assume that the diodes are standard silicon, with each modeled as possessing a current-independent conduction voltage of 0.7 V. We assume the MOSFETs have a drain–source

Table 1. H-bridge electronic parameters for example.

Variable	Value
R_0	140 mΩ
V_0	1.4 V
τ_s	40 ns
U_g	30 nJ
L	10 μH

impedance that is resistive, with a value of 45 mΩ when gated with gate-source voltage of 1.5 V. For the inductor, we take its inductance to be $L = 10\,\mu\text{H}$, which is rather small but not atypical for a discontinuously conducting H-bridge. We assume the inductor has an effective series resistance of 50 mΩ. Thus, the total conductive loss parameters for the H-bridge are taken to be $V_0 = 2\times 0.7 = 1.4\text{V}$ and $R_0 = 2\times 45 + 50 = 140\,\text{m}\Omega$. We take the MOSFET transition time to be 40 ns. For the gating energy, we assume that the MOSFETs have a gate capacitance of 10 nC, resulting in an idealized gating energy of $\frac{1}{2}\times 10\,\text{nC}\times(1.5\text{V})^2 = 7.5\,\text{nJ}$ each. To account for nonlinear electrical phenomena (i.e. Miller effects), we multiply this energy by a factor of 2, to obtain an effective gating energy of 15 nJ each. As each switching cycle gates two MOSFETs, we arrive at a total gating energy of $U_g = 30\,\text{nJ}$.

We will not specify V_S and f_s, but instead will vary these two quantities to see how $\bar{P}_{gen}$ depends on them.

As competing constraints impinging on control design, we first use the pole placement constraint to ensure that the dynamics of the closed-loop system are at frequencies at least a decade below the switching frequency. Consequently, we set

$$\omega_0 = \tfrac{2\pi}{10} f_s \tag{104}$$

For the time being, we will not enforce any constraint on the closed-loop damping, that is, $\zeta_0 = 0$. We must also impose a constraint such that voltage bound, as in equation (88). In this example, we will uniformly set $\delta = 2$. This will be the only competing dynamic objective for the example, so we have that $z = v$ and $\gamma = V_S^2/4$.

We first illustrate the way the value of $\bar{P}^{\star}_{gen}$, evaluated with the optimized controller parameters, varies with V_S and f_s. This is illustrated in Figure 5 for σ_a values of 0.2, 0.5, and 1 g. Note that in all three cases, there is an optimum, finite switching frequency, and bus voltage. If the bus voltage is too small, it hampers the controller by requiring the transducer voltage to be suppressed, per the voltage constraint (88). Meanwhile, if the bus voltage is too large, transition losses and average i^2R losses in μ increase, per equation (95). Similarly for f_s, if it is too small, this hampers performance in multiple ways. It restricts the pole placement constraint (104) and also increases transition and resistive losses by increasing current ripple amplitudes. Meanwhile, if f_s is too large, the gating losses become prohibitive.

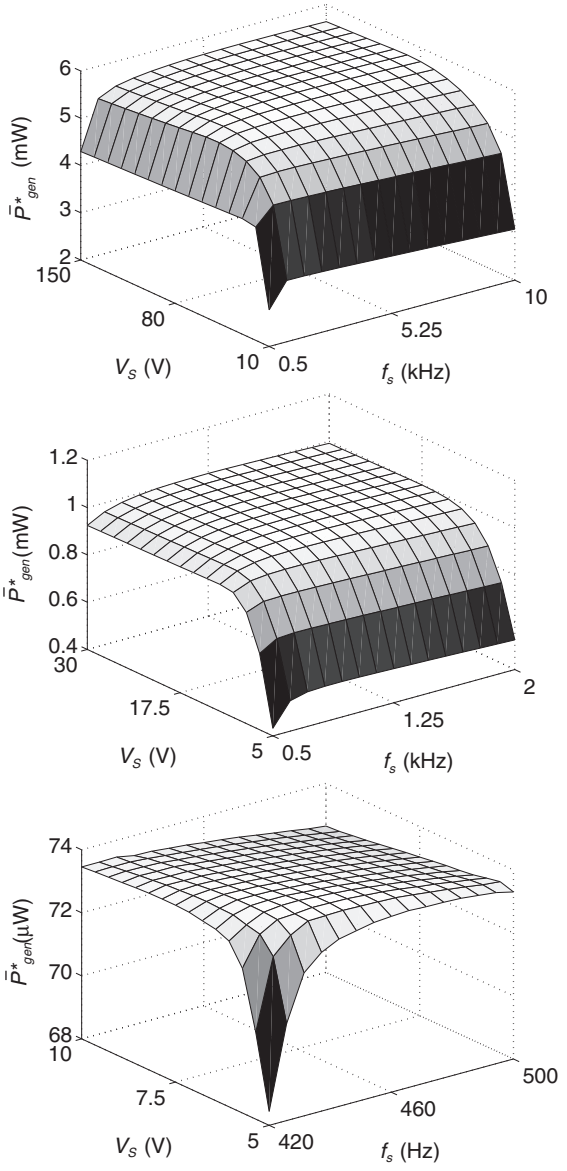

Figure 5. Surface plots for $\bar{P}^{\star}_{gen}$ as a function of $\{V_S, f_s\}$, for $\sigma_a = 1$ g (top), $\sigma_a = 0.5$ g (middle), and $\sigma_a = 0.2$ g (bottom).

To better illustrate the optimal combinations of $\{f_s, V_S\}$, and their dependency on σ_a, Figure 6 shows this dependency explicitly. As shown, V_S appears to increase in a manner that is approximately quadratic with σ_a. Meanwhile, f_s increases in a manner that is almost linear, except near $\sigma_a = 0.7$ g, where the slope changes. Note that at $\sigma_a = 0.2$, the optimal f_s is very low, at 432 Hz (i.e. at approximately $10\omega_a/2\pi$). The optimal value of f_s can never be below this value, because the disturbance model is uncontrollable, and thus, it is impossible to place the closed-loop poles of the disturbance model. This implies that $\omega_0 > \omega_a$ is always required, for the problem as stated in this article.

Now, we modify our example by setting ζ_0 to a value greater than zero. For ζ_0 sufficiently large, this will force the controller optimization to sacrifice

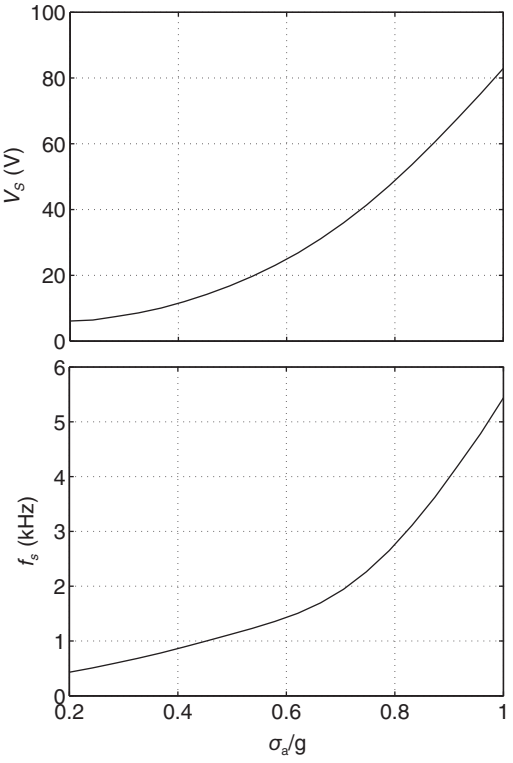

Figure 6. Optimal $\{V_S, f_s\}$ combinations, with simultaneously optimized feedback, as a function of σ_a.

performance (i.e. $\bar{P}_{gen}$) in order to enhance the damping of the closed-loop system. As such, as ζ_0 is increased, it is possible to illustrate the trade-off that must be struck between the energy harvesting objective and competing structural control (i.e. damping) objectives.

The plots in Figure 7 illustrate this trade-off for σ_a values of 0.2, 0.5, and 1 g. In each case, the optimal $\{f_s, V_S\}$ values for $\zeta_0 = 0$ were used. Each plot shows both the actual value of $\bar{P}^{\star}_{gen}$, and the conservative lower bound as in equation (100). Recall that the lower bound on $\bar{P}_{gen}$ is actually the quantity that is maximized, subject to the damping constraint. As such, it is not surprising that in all cases, this quantity decreases monotonically as ζ_0 is increased, dropping sharply for ζ_0 values above about 0.03. It is also not surprising that the actual value of $\bar{P}^{\star}_{gen}$ is slightly above this bound. However, it is not necessarily the case that the actual $\bar{P}^{\star}_{gen}$ value decreases monotonically as the damping constraint is tightened, because it is not this actual value that is optimized for a given ζ_0 but rather only its lower bound. The domain of ζ_0 values for each plot constitutes the range of values for which all the constraints of the problem have a feasible solution. In other words, for ζ_0 values in excess of that of the maximum data point for each plot, the optimization problem becomes infeasible. In such cases, it is impossible to provide the desired level of damping (irrespective of the suboptimality of $\bar{P}_{gen}$) while also keeping voltage magnitudes

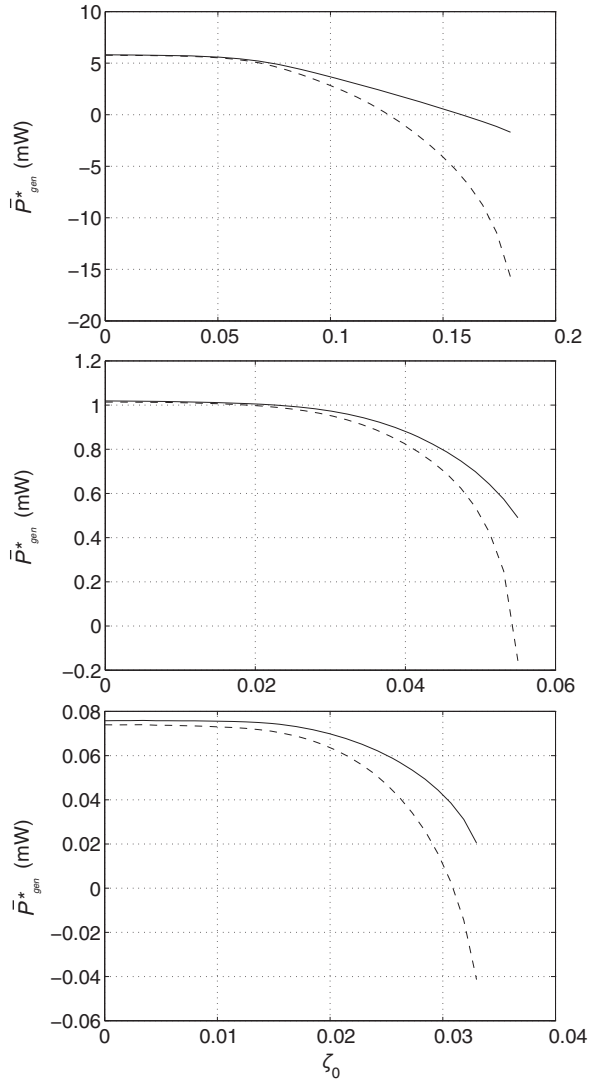

Figure 7. Values of $\bar{P}^{\star}_{gen}$ (solid) and its optimized lower bound (dotted) as a function of damping constraint ζ_0. The three plots are for $\{\sigma_0, V_S, f_s\}$ values of {1 g, 83 V, 5.4 kHz} (top), {0.5 g, 17 V, 1.1 kHz} (middle), and {0.2 g, 6.1 V, 432 Hz} (bottom).

sufficiently low and keeping the eigenvalues at moduli below ω_0. As such, these plots illustrate that for given hardware parameters and given V_S and f_s, it is possible to find the maximum structural damping that can be provided with this configuration.

Conclusion

This article has illustrated that through the use of LMI techniques, feedback controllers for active stochastic energy harvesting can be designed, which maximize average power generation, subject to other closed-loop requirements. These requirements may arise due to operating conditions, which must be sustained for the electronics to be controlled. They may also arise due to

the dual functionality of a transduction system for both energy harvesting and structural control. The analysis leading to Figure 7 illustrates a central feature of the feedback optimization approach to energy harvesting illustrated in this article. It can be used to explicitly balance energy harvesting against structural control objectives, in the context of broadband stochastic vibrations. In our analysis, these structural control objectives manifest themselves as a constraint on the damping of the closed-loop system. However, as illustrated in Scherer et al., (1997), many other types of control objectives, including $\mathcal{H}_2$ and $\mathcal{H}_\infty$ performance objectives, peak-to-peak gain bounds, overshoot bounds, tracking objectives, and robustness objectives can be addressed in very much the same manner.

Additionally, this article has illustrated that the optimal active control theory proposed in prior work, which assumed quadratic (i.e. resistive) transmission loss models, can be extended to accommodate more realistic but nonquadratic loss models, such as those that manifest themselves in active drive circuits. With more realistic loss models, it becomes clearer how various parameters reflecting the operation of the active electronics (such as bus voltages and switching frequencies) affect the optimal feedback law, as well as the optimal performance achieved. These more detailed models also allow us to determine the sensitivity of power generation (and control design) to various hardware parameters in the electronics, such as gating energies, switch transition times, diode conduction voltages, and resistances.

Although we have illustrated these concepts in the context of discontinuously conducting active H-bridge drives, similar loss models and resultant analyses might be conducted for other linearly controlled active harvesting circuits. However, the convergence of the algorithm outlined in problem *OP*3 is only guaranteed if the loss model has the semiconcave property, and this property may not hold for all systems.

In many applications, the power scale is low enough that the use of an active drive such as the one considered here cannot be justified, when compared against performance with passive circuits, or low-frequency-switched approaches such as SSHI circuits. However, it is anticipated that by solving feedback optimizations for the linear case, techniques may be developed, which extend these methods to other, nonlinearly constrained harvesting circuits. Extensions along these lines have recently been proposed by the authors (Scruggs and Cassidy, 2010), for the case of single-directional converters such as that in Figure 2(b), with controllable duty cycle.

One interesting open problem that is left unanswered by the present analysis concerns the development of techniques for simultaneous energy harvesting and system stabilization. Indeed, the theory that has been proposed here breaks down when the harvester is not passive, which rules out open-loop unstable harvesters. This also excludes all stable harvesters with driving point impedances that contain internal energy sources, such as harvesters with parametric excitations. In such cases, competing response objectives in the control design would be necessary, because otherwise the optimal controller would be destabilizing.

Funding

The first two authors gratefully acknowledge support for this research, through NSF grant CMMI-0747563. The views expressed in this article are those of the authors and do not necessarily reflect those of the National Science Foundation.

References

Adhikari S, Friswell M and Inman DJ (2009) Piezoelectric energy harvesting from broadband random vibrations. *Smart Materials and Structures* 18: 115005.

Amirtharajah R and Chandrakasan AP (1998) Self-powered signal processing using vibration-based power generation. *IEEE Journal of Solid-State Circuits* 33: 687–695.

Anton SR and Sodano HA (2007). A review of power harvesting using piezoelectric materials (2003–2006). *Smart Materials and Structures* 16: R1–R21.

Badel A, Guyomar D, Lefeuvre E, et al. (2005) Efficiency enhancement of a piezoelectric energy harvesting device in pulsed operation by synchronous charge inversion. *Journal of Intelligent Material Systems and Structures* 16: 889–901.

Beeby SP, Tudor MJ and White NM (2006) Energy harvesting vibration sources for microsystems applications. *Measurement Science and Technology* 17: R175–R195.

Boyd S, El Ghaoui L, Feron E, et al. (1994) *Linear Matrix Inequalities in System and Control Theory*. Philadelphia, PA: SIAM.

Brogliato B, Lozano R, Maschke B, et al. (2007) *Dissipative Systems Analysis and Control*. 2nd ed. London: Springer-Verlag.

Cammarano A, Burrow SG, Barton DAW, et al. (2010) Tuning a resonant energy harvester using a generalized electrical load. *Smart Materials and Structures* 19: #055003.

Cassidy IL, Scruggs JT and Behrens S (2011). Design of electromagnetic energy harvesters for large-scale structural vibration applications. In: *SPIE international symposium on smart materials and structures/NDE*, San Diego, CA, 6–10 March.

Chilali M and Gahinet P (1996) H_∞ design with pole placement constraints: an LMI approach. *IEEE Transactions on Automatic Control* 41: 358–367.

Cruz J (ed.) (2008) *Ocean Wave Energy: Current Status and Future Perspectives*. Berlin: Springer-Verlag.

Daqaq MF (2011) Transduction of bistable inductive generator driven by white and exponentially correlated Gaussian noise. *Journal of Sound and Vibration* 330: 2554–2564.

Guyomar D, Badel A, Lefeuvre E, et al. (2005) Toward energy harvesting using active materials and conversion improvement by nonlinear processing. *IEEE Transactions on Ultrasonics, Ferroelectrics, and Frequency Control* 52: 584–595.

Halvorsen E (2009) Energy harvesters driven by broadband random vibrations. *Journal of Microelectromechanical Systems* 17(5): 1061–1071.

Kasyap A, Lim J, Johnson D, et al. (2002). Energy reclamation from a vibrating piezoceramic composite beam. In: *Ninth international congress on sound and vibration*, Orlando, FL, 8–11 July.

Kong N, Ha DS, Erturk A, et al. (2010) Resistive impedance matching circuit for piezoelectric energy harvesting. *Journal of Intelligent Material Systems and Structures* 21: 1293–1302.

Lefeuvre E, Audigier D, Richard C, et al. (2007) Buck-boost converter for sensorless power optimization of piezoelectric energy harvester. *IEEE Transactions on Power Electronics* 22: 2018–2025.

Lefeuvre E, Badel A, Richard D, et al. (2005) Piezoelectric energy harvesting device optimization by synchronous electric charge extraction. *Journal of Intelligent Material Systems and Structures* 16: 865–876.

Lesieutre GA, Ottman GK and Hofmann HF (2004) Damping as a result of piezoelectric energy harvesting. *Journal of Sound and Vibration* 269: 991–1001.

Liang JR and Liao WH (2009) Piezoelectric energy harvesting and dissipation on structural damping. *Journal of Intelligent Material Systems and Structures* 20: 515–527.

Liang JR and Liao WH (2011) On the influence of transducer internal loss in piezoelectric energy harvesting with SSHI interface. *Journal of Intelligent Material Systems and Structures* 22: 503–512.

Lien IC, Shu YC, Wu WJ, et al. (2010) Revisit of series-SSHI with comparisons to other interfacing circuits in piezoelectric energy harvesting. *Smart Materials and Structures* 19: 125009.

Liu Y, Tian G, Wang Y, et al. (2009) Active piezoelectric energy harvesting: general principle and experimental demonstration. *Journal of Intelligent Material Systems and Structures* 20: 575–585.

Luo C and Hofmann HF (2011) Wideband energy harvesting for piezoelectric devices with linear resonant behavior. *IEEE Transactions on Ultrasonics, Ferroelectrics, and Frequency Control* 58(7): 1294–1301.

Nagode C, Ahmadian M and Taheri S (2010). Feasibility study of passive electromagnetic damping systems. In: *SPIE international symposium on smart materials and structures/NDE*, San Diego, CA, 7–11 March.

Ottman GK, Hofmann HF and Lesieutre GA (2003) Optimized piezoelectric energy harvesting circuit using step-down converter in discontinuous conduction mode. *IEEE Transactions on Power Electronics* 18: 696–703.

Priya S and Inman DJ (eds) (2009) *Energy Harvesting Technologies*. New York: Springer.

Roundy S, Wright PK and Rabaey J (2002) A study of low level vibrations as a power source for wireless sensor nodes. *Computer Communications* 26: 1131–1144.

Scherer C, Gahinet P and Chilali M (1997) Multiobjective output-feedback control via LMI optimization. *IEEE Transactions on Automatic Control* 42: 896–911.

Scruggs JT (2009) An optimal stochastic control theory for distributed energy harvesting networks. *Journal of Sound and Vibration* 320: 707–725.

Scruggs JT (2010) On the causal power generation limit for a vibratory energy harvester in broadband stochastic response. *Journal of Intelligent Material Systems and Structures* 21: 1249–1262.

Scruggs JT and Cassidy IL (2010). Optimal and sub-optimal power management in broadband vibratory energy harvesters with one-directional power flow constraints. In: *SPIE international symposium on smart materials and structures/NDE*, San Diego, CA, 7–11 March.

Shu YC and Lien IC (2006) Analysis of power output for piezoelectric energy harvesting systems. *Smart Materials and Structures* 15: 1499–1512.

Sodano HA, Park G and Inman DJ (2004) Estimation of electric charge output for piezoelectric energy harvesting. *Strain* 40: 49–58.

Stephen NG (2006) On energy harvesting from ambient vibration. *Journal of Sound and Vibration* 293: 409–425.

Tang L, Yang Y and Soh CK (2010) Toward broadband vibration-based energy harvesting. *Journal of Intelligent Material Systems and Structures* 21: 1867–1897.

Taylor GW, Burns JR, Kammann SA, et al. (2001) The energy harvesting Eel: A small subsurface ocean/river power generator. *IEEE Journal of Oceanic Engineering* 26: 539–547.

Wickenheiser AM and Garcia E (2010) Power optimization of vibration energy harvesters using passive and active circuits. *Journal of Intelligent Material Systems & Structures* 21: 1343–1361.

Zuo L, Scully B, Shestani J, et al. (2010) Design and characterization of an electromagnetic energy harvester for vehicle suspensions. *Smart Materials and Structures* 19: